Engineering Notes

Establishment of Natural Solar Sail Formation Using Solar Electric Propulsion

Khashayar Parsay* and Hanspeter Schaub†
University of Colorado, Boulder, Colorado 80309

DOI: 10.2514/1.G001479

Nomenclature

a	=	semimajor axis, km
a_r, a_θ, a_h	=	solar radiation pressure acceleration along radial, along-track, and cross-track directions, km/s^2
$\boldsymbol{a}_s$	=	solar radiation pressure acceleration, km/s^2
$\boldsymbol{a}_{\eth}$	=	acceleration due to Earth's nonsphericity, km/s^2
$\boldsymbol{a}_{\mathbb{C}}$	=	acceleration due to moon's gravity, km/s^2
$\boldsymbol{a}_{\odot}$	=	acceleration due to sun's gravity, km/s^2
$[\boldsymbol{C}_i]$	=	rotation matrix about i axis
e	=	eccentricity
f	=	true anomaly, deg
i	=	inclination, deg
J	=	cost function
k	=	characteristic acceleration of solar sail, km/s^2
$\mathcal{N}$	=	Earth-centered ecliptic inertial frame
$[\mathcal{NO}]$	=	direction cosine matrix that transfers vector from $\mathcal{O}$ to $\mathcal{N}$ frame
$\hat{\boldsymbol{n}}_s$	=	sun-line unit vector
$\hat{\boldsymbol{n}}$	=	sail normal unit vector
$\mathcal{O}$	=	local-vertical–local-horizontal frame
R_E	=	Earth's radius, km
$\boldsymbol{r}$	=	sail position vector, km
T	=	orbit period, s
$\hat{\boldsymbol{T}}$	=	unit thrust direction
V	=	local-velocity-normal-binormal frame
$\delta\text{œ}$	=	differential orbital elements
λ_s	=	sun longitude measured from vernal equinox, deg
μ	=	Earth's gravitational constant, km^3/s^2
Ω	=	right ascension of ascending node, deg
ω	=	argument of perigee, deg
œ	=	array containing classical orbital elements $[a, e, i, \Omega, \omega, f]^T$

Subscripts

c	=	chief solar sail
d	=	deputy solar sail

Received 15 May 2015; revision received 11 October 2015; accepted for publication 17 October 2015; published online 29 December 2015.

*Doctoral Student, Aerospace Engineering Sciences Department.
†Professor, Aerospace Engineering Sciences Department.

I. Introduction

SOLAR sail low-thrust propulsion is capable of achieving long residence in the geomagnetic tail by continuously precessing the orbit apse line. McInnes et al. [1–3] propose the low-cost GEOSAIL mission to explore the Earth's magnetosphere using a single low-performance solar sail. In the GEOSAIL mission, the solar sail would fly in a moderately elliptical orbit that lies in the ecliptic plane and would employ a simple sun-pointing steering law to precess the orbit apse line sun synchronously, allowing the orbit apogee to remain in the geomagnetic tail throughout the entire year. Many magnetosphere missions require more than a single spacecraft to achieve their scientific objective. NASA's Time History of Events and Macroscale Interactions during Substorms and Magnetospheric Multi-Scale missions along with ESA's Cluster II mission are some of the currently active magnetosphere missions requiring multiple spacecraft to accomplish their scientific objectives [4]. Gong et al. [5] propose solar sail formation flying for exploring the geomagnetic tail. In [5], the chief solar sail employs a sun-synchronous orbit, while the deputy solar sail uses active control to enable close-proximity formation flying. Mu et al. [6] expand the work in [5] by applying two nonlinear-based control laws that use reflectivity modulation for enforcing a projected-circular relative motion. The coupled control of a reflectivity modulated solar sail formation is discussed by Mu et al. in [7]. The results indicate that it is difficult to control the solar sail's attitude and orbit simultaneously using reflectivity modulation. Natural solar sail formations for GEOSAIL formation flying are proposed in [8]. An analytic condition for determining target states that lead to in-plane quasi-periodic relative motion under solar radiation pressure is derived, assuming all sails use the same sun-pointing steering law for precessing their orbit apse lines.

The problem of formation deployment and the establishment of a desired relative geometry for GEOSAIL formation flying has yet to be explored in the literature. In this Note, a natural leader–follower formation is established using a hybrid system that combines solar sailing with solar electric propulsion (SEP). The main advantage of a natural leader–follower formation is that it only requires the sails to maintain a sun-pointing attitude once the desired relative motion is achieved via the SEP system. The two sails employ the sun-pointing attitude to precess their orbit apse lines sun synchronously. The chief is assumed to be a low-cost solar sail that only maintains a sun-pointing attitude, while the deputy is a hybrid system with a small SEP thruster. The problem of deployment and the establishment of the natural formation using low-thrust one-burn and two-burn maneuver strategies are discussed in detail. Because the SEP system is unable to fire thrusters in the direction of the sail's reflective surface, the formation establishment problem is a constrained two-point boundary value problem (TPBVP). This constrained two-point boundary value problem is solved numerically using a predictor-corrector method. A Monte Carlo analysis is performed to study the solution space for the problem of formation establishment when the two sails are inserted into slightly different mission orbits due to the launcher's attitude error. The effects of Earth's nonsphericity, lunar gravity, and solar gravity are included in all the simulations to ensure a high-fidelity analysis.

II. Equations of Motion of Solar Sails in Earth Orbits

The general equations of motion for a solar sail in an Earth orbit is written as

$$\ddot{\boldsymbol{r}} = -\frac{\mu}{r^3}\boldsymbol{r} + \boldsymbol{a}_{\eth} + \boldsymbol{a}_{\mathbb{C}} + \boldsymbol{a}_{\odot} + \boldsymbol{a}_s \tag{1}$$

where $\boldsymbol{r}$ is the position vector of the spacecraft relative to the Earth and $\boldsymbol{a}_{\eth}$, $\boldsymbol{a}_{\mathbb{C}}$, $\boldsymbol{a}_{\odot}$, and $\boldsymbol{a}_s$ are the accelerations due to Earth's nonsphericity, lunar gravitational effects, solar gravitational effects,

and solar radiation pressure, respectively. The adopted inertial frame $\mathcal{N} = \{O, \boldsymbol{X}, \boldsymbol{Y}, \boldsymbol{Z}\}$ has its origin O at the center of the Earth where the x axis points from the origin to the equinox and z points along the ecliptic north pole. The y axis completes the right-handed coordinate system. For a flat, rigid, perfectly reflecting solar sail, the solar sail's acceleration due to the Solar Radiation Pressure (SRP) can be written as [1]

$$\boldsymbol{a}_s = k(\hat{\boldsymbol{n}}_s \cdot \hat{\boldsymbol{n}})^2 \hat{\boldsymbol{n}} \tag{2}$$

where $\hat{\boldsymbol{n}}$ is a unit vector normal to the sail surface, $\hat{\boldsymbol{n}}_s$ is a unit vector from the sun to the Earth, and the parameter k is the sail's characteristic acceleration. For the GEOSAIL mission, McInnes et al. [1–3] propose flying a solar sail in the ecliptic plane using a simple steering law consisting of the sail's normal vector continuously pointing along the sun line within the orbit plane such that the rotation of the orbit apse line is synchronous with the annual rotation of the sun line. The sun-synchronized precession of the orbit apse line allows the orbit apogee to remain in the geomagnetic tail continuously, thus enabling science data collection for long periods. The required characteristic acceleration k to precess the orbit sun synchronously is dependent on the shape of the orbit and is computed according to [1,2]

$$k(a, e) = \frac{2}{3}\dot{\lambda}_s \frac{e}{\sqrt{1-e^2}}\sqrt{\frac{\mu}{a}} \tag{3}$$

As shown in Fig. 1a, the SRP acceleration ${}^{\mathcal{O}}\boldsymbol{a}_s$ expressed in the sail's local-vertical–local-horizontal (LVLH) frame may be written as

$${}^{\mathcal{O}}\boldsymbol{a}_s = k(\hat{\boldsymbol{n}}_s \cdot \hat{\boldsymbol{n}})^2 {}^{\mathcal{O}}\hat{\boldsymbol{n}} = {}^{\mathcal{O}}\begin{bmatrix} a_r \\ a_\theta \\ a_h \end{bmatrix} = {}^{\mathcal{O}}\begin{bmatrix} k\cos\alpha\cos\phi \\ k\cos\alpha\sin\phi \\ -k\sin\alpha \end{bmatrix} \tag{4}$$

For the LVLH frame $\mathcal{O} = \{o, \hat{\boldsymbol{o}}_r, \hat{\boldsymbol{o}}_\theta, \hat{\boldsymbol{o}}_h\}$, $\hat{\boldsymbol{o}}_r$ points along the sail's position vector, $\hat{\boldsymbol{o}}_h$ is directed along the orbit angular momentum vector, and $\hat{\boldsymbol{o}}_\theta = \hat{\boldsymbol{o}}_h \times \hat{\boldsymbol{o}}_r$ completes the right-handed coordinate system. As illustrated in Fig. 1b, the sail's normal $\hat{\boldsymbol{n}}$ points along the sun line within the ecliptic plane such that the identity $\omega = \lambda_s$ and $\hat{\boldsymbol{n}} \cdot \hat{\boldsymbol{n}}_s = 1$ hold. This leads to the orbit apse line always pointing along the sun line $\hat{\boldsymbol{n}}_s$. The sail's sun-pointing attitude leads to having $\phi = \pi - f$ and $\alpha = 0$. Substituting these identities to Eq. (4), the sail's normal vector becomes ${}^{\mathcal{O}}\hat{\boldsymbol{n}} = {}^{\mathcal{O}}[-\cos f \quad \sin f \quad 0]^T$. The direction cosine matrix $[\mathcal{NO}] = [{}^{\mathcal{N}}\hat{\boldsymbol{o}}_r \quad {}^{\mathcal{N}}\hat{\boldsymbol{o}}_\theta \quad {}^{\mathcal{N}}\hat{\boldsymbol{o}}_h]$ is used to transfer the sail's normal ${}^{\mathcal{O}}\hat{\boldsymbol{n}}$ from the reference frame $\mathcal{O}$ to the inertial frame $\mathcal{N}$ to be used in Eq. (1). The sunlight direction expressed in the inertial frame $\mathcal{N}$ is ${}^{\mathcal{N}}\hat{\boldsymbol{n}}_s = {}^{\mathcal{N}}[-\cos\lambda_s \quad -\sin\lambda_s \quad 0]^T$, where the longitude of the sun λ_s is determined through $\lambda_s = \lambda_{s_0} + \dot{\lambda}_s t$.

Another local reference frame used in this Note is the velocity-normal-binormal frame $\mathcal{V} = \{o, \hat{\boldsymbol{o}}_v, \hat{\boldsymbol{o}}_h, \hat{\boldsymbol{o}}_b\}$, where $\hat{\boldsymbol{o}}_v$ points along the local velocity direction, $\hat{\boldsymbol{o}}_h$ is directed along the orbit angular momentum vector, and $\hat{\boldsymbol{o}}_b = \hat{\boldsymbol{o}}_v \times \hat{\boldsymbol{o}}_h$ completes the right-handed coordinate system.

The mission orbit considered is an $11\,R_E \times 30\,R_E$ orbit that lies in the ecliptic plane. The corresponding orbit period is $T = 5.4457$ days. The orbital elements for the mission orbit are $a = 130,751.8$ km, $e = 0.4634$, $i = 0$ deg, $\omega = 0$ deg, and $\Omega = 0$ deg.

Although a hybrid sail enables the establishment of formation geometries that may not be possible with a solar sail alone, the design of such a system is significantly more difficult. With the additional mass of the SEP system, the required reflective surface area must increase in order to maintain the required characteristic acceleration given in Eq. (3) for sun-synchronous precession of the orbit apse line. The main advantage of the SEP system is that the thrust value is known upfront and is accurately estimated on the ground, unlike a solar sail for which the exact value of the sail's characteristic acceleration model is difficult to estimate [9]. Furthermore, the SEP system is more reliable in terms of generating the required acceleration since it is not prone to the physical issues that a sail's reflective surface is prone to, such as degradation, wrinkles, and a large uncertainty of the optical properties. Because the natural formation requires no formation maintenance, the SEP system is primarily used for establishing the desired formation. This allows for the selection of a small SEP system, leading to only a small increase in solar sail mass and reflective surface area. The required characteristic acceleration to precess the apse line of an $11\,R_E \times 30\,R_E$ orbit sun synchronously is $k = 0.12119$ mm/s^2. Assuming a constant solar radiation of $P = 4.56 \times 10^{-6}$ N/m^2 and solar sail efficiency of $\eta = 0.85$, the required sail loading $\sigma = 2\eta P/k = m_0/A_s$ for generating the characteristic acceleration of $k = 0.12119$ mm/s^2 is 63.96 g/m^2. The total mass of the hybrid system is computed to be $m_0 = 120$ kg, assuming only

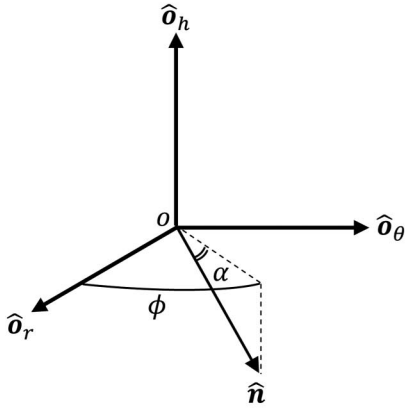

a) Sail's normal vector orientation in the LVLH frame

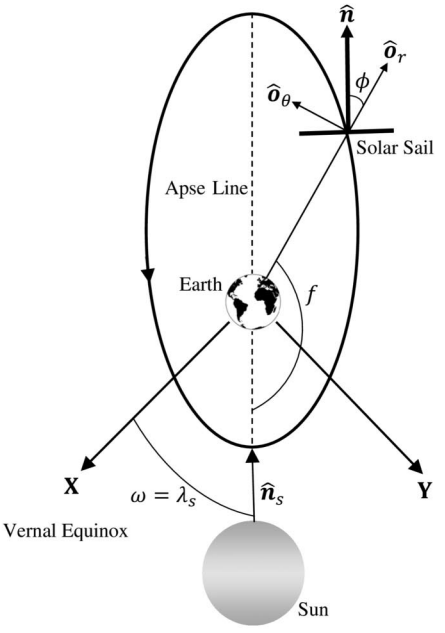

b) Sail's orbit geometry

Fig. 1 Sail's orbit geometry and general orientation.

0.5 kg for the propellant mass. This crude mass estimation is based on [10] and [11]. For a hybrid sailcraft with a total launch mass of $m_0 = 120$ kg, a reflectable area of $A_s \approx 1876$ m^2 is required for generating the computed sail loading. The total surface area of the sail is computed using $A = A_s + A_{\text{cells}}$, where A_{cells} is a small area (5% of the total area) covered with thin film solar cells used to provide power for the SEP system. The SEP system is assumed to be able to generate the maximum thrust of $T_{\max} = 0.01$ N with $I_{\text{SP}} = 2500$ s. Such a SEP system falls within the scope of current technology [12]. For a typical square sail configuration, the size of the sail is approximately 44×44 m.

III. Natural Leader–Follower Formation

In this section, a natural formation is proposed for flying two solar sails in a leader–follower formation in an eccentric orbit. It is assumed that both solar sails always point toward the sun line to individually precess their orbit apse line sun synchronously. The goal is to maintain a formation without continuously varying the sail's orientation or changing the sail's reflectivity. Let $\mathfrak{oe}_{d_0}$ and $\mathfrak{oe}_{c_0}$ denote the initial classical osculating orbital elements for the deputy and chief solar sails, respectively. The differential orbital elements are defined as $\delta\mathfrak{oe}_0 = \mathfrak{oe}_{d_0} - \mathfrak{oe}_{c_0} = [\,\delta_{a_0} \quad \delta_{e_0} \quad \delta_{i_0} \quad \delta_{\Omega_0} \quad \delta_{\omega_0} \quad \delta_{f_0}\,]^T$. A natural leader–follower formation may be established if the following initial differential orbital elements are established at orbit apogee:

$$\delta\mathfrak{oe}_0 = [\,0 \quad 0 \quad 0 \quad 0 \quad 0 \quad \delta f_0\,]^T \tag{5}$$

If the chief is in a circular orbit, the deputy holds a constant offset behind or ahead of the chief throughout the entire orbit, depending on the sign of δf_0. For a chief in an eccentric orbit, the deputy's relative motion is a bounded periodic motion that takes place behind the chief if $\delta f_0 < 0$ and ahead of the chief if $\delta f_0 > 0$ and satisfies the condition

$$\frac{\dot{y}(t_0)}{x(t_0)} = \frac{-n(2-e)}{\sqrt{(1-e)(1+e)^3}} \tag{6}$$

at orbit apogee [13], where n and e are the chief's mean motion and eccentricity, respectively. The formation size is only dependent on the magnitude of δf_0. An example of such relative motion is illustrated in Fig. 2 for two different formation sizes of $\delta f_0 = -0.001$ deg and $\delta f_0 = -0.01$ deg. The minimum and maximum distances between the chief and deputy sails occur at the chief's apogee and perigee, respectively. The minimum distance can be analytically computed using the along-track equation $y \approx r_c(\delta f + \delta\omega + \delta\Omega \cos i)$ [14].

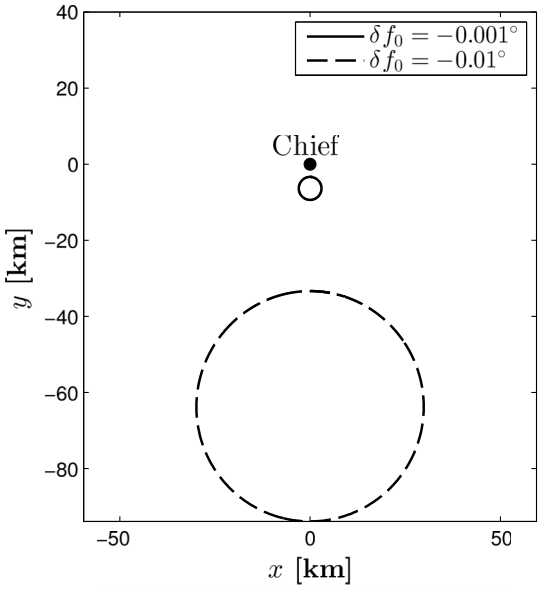

Fig. 2 Deputy's relative motion in the chief's LVLH frame for various true anomaly offsets.

Since $\delta\omega = \delta\Omega = 0$, the minimum distance is determined as $y_{\min} = r_c\delta f$. To determine the center and the radius of the relative circular orbit, the relative motion is propagated for a full orbit, and a least-squares solution is used to fit a circle to the deputy's relative motion. Let (x_o, y_o) and R denote the center and the radius of the relative circular motion of the deputy. To determine (x_o, y_o) and R, the problem

$$\text{minimize } J = \sum_{i=1}^{N} [(x_i - x_{\text{o}})^2 + (y_i - y_{\text{o}})^2 - R^2]^2$$
$$\text{with respect to } x_{\text{o}}, y_{\text{o}}, R \tag{7}$$

must be solved, where N is the number of integration steps taken in propagating the formation for one full orbit. This minimization problem may be converted to a simple least-squares problem by a change of variables. Expanding the cost function leads to

$$J = \sum_{i=1}^{N} (x_i^2 - 2x_i x_o + y_i^2 - 2y_i y_o + w)^2$$

where $w = x_o^2 + y_o^2 - R^2$ is used as a new variable. Let $\boldsymbol{\epsilon} = \boldsymbol{A}\boldsymbol{x} - \boldsymbol{b}$, where

$$\boldsymbol{A} = \begin{bmatrix} -2x_1 & -2y_1 & 1 \\ -2x_2 & -2y_2 & 1 \\ \vdots & \vdots & \vdots \\ -2x_N & -2y_N & 1 \end{bmatrix}, \quad \boldsymbol{x} = \begin{bmatrix} x_o \\ y_o \\ w \end{bmatrix}, \quad \boldsymbol{b} = -\begin{bmatrix} x_1^2 + y_1^2 \\ x_2^2 + y_2^2 \\ \vdots \\ x_N^2 + y_N^2 \end{bmatrix}$$

Hence, the cost function in Eq. (7) may now be rewritten as $J = \|\boldsymbol{\epsilon}\|_2^2$. The center and the radius of the circular relative motion are found using the least-squares solution $\boldsymbol{x} = (\boldsymbol{A}^T\boldsymbol{A})^{-1}\boldsymbol{A}^T\boldsymbol{b}$. The radius of the relative circular orbit is solved using $R = \sqrt{x_o^2 + y_o^2 - w}$. For the $\delta f_0 = -0.001$ deg case shown in Fig. 2, the center and the orbit radius of the deputy's relative motion are $(x_o, y_o) = (0, -6.33)$ km and $R = 2.98$ km. For the formation size $\delta f_0 = -0.001$ deg, they are $(x_o, y_o) = (0, -63.3)$ km and $R = 29.8$ km. The formation stability of the natural leader–follower formation under gravitational and SRP perturbations is examined for a formation established using $\delta_0 = [\,0 \quad 0 \quad 0 \quad 0 \quad 0 \quad -0.001\,]^T$. The simulation is generated for two different periods as illustrated in Fig. 3. The relative out-of-plane motion degrades, but the effect is negligible, with a maximum out-of-plane separation of only 9 m. The formation remains quasi-periodic even after six months, despite the secular drift in the along-track direction. In reality, the achievement of the desired differential elements is bound to have small errors. Thus, formation reconfiguration is necessary after a few months.

IV. Sails Deployment into Mission Orbit

In this section, formation deployment into the GEOSAIL mission orbit is discussed. This analysis is necessary for an accurate modeling of the formation establishment problem. It is assumed that a dedicated launcher releases the two solar sails directly into the $11\,R_E \times 30\,R_E$ mission orbit. Note that to obtain the GEOSAIL mission orbit an auxiliary upper stage is required, regardless of the selected launch vehicle. The requirement for the two sails to be injected directly into the mission orbit narrows down the launch vehicle options and increases mission cost. However, in terms of flight dynamics, it is the most realistic option since the alternative would require injecting the sails into lower orbits and performing orbit raising to achieve the GEOSAIL mission orbit.

The two sails are released sequentially within the orbit plane at the perigee of the operational mission orbit. Because the desired natural formation is an in-plane relative motion, the deployment must be conducted within the orbit plane, since correcting the out-of-plane differential elements δi and $\delta\Omega$ is difficult even for a hybrid solar sail with a SEP system. The chief is released along the local velocity

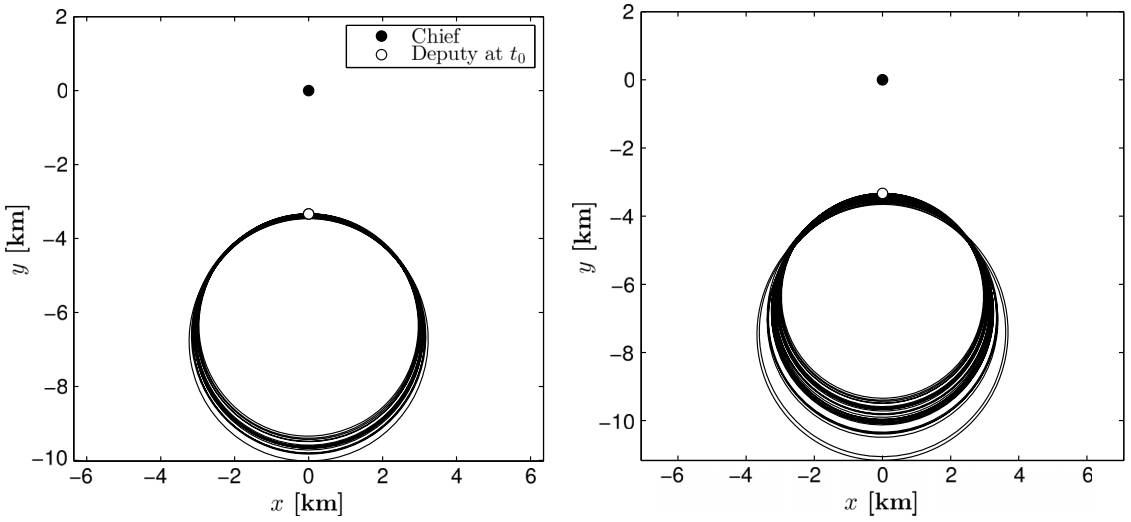

a) 3 months **b) 6 months**

Fig. 3 Deputy's relative motion in the chief's LVLH xy plane under perturbations.

direction. The deputy sail is released in a slightly different direction than the velocity to avoid close approaches. In this study, the deputy is assumed to be released along a direction that is 1 deg off the local velocity direction while lying within the orbit plane. The springs used in deploying the sails are assumed to be capable of generating an impulsive velocity change of 5 m/s relative to the auxiliary upper stage. This value is a conservative value that is one order of magnitude higher than the minimum requirement for the launch vehicle upper stage [15]. Thus, upon deployment, the impulsive velocity changes for the chief and deputy sails expressed in the $\mathcal{V}$ frame are ${}^{\mathcal{V}}\Delta\boldsymbol{v}_c = [\,\Delta v_v \quad \Delta v_h \quad \Delta v_b\,]^T = [\,5 \quad 0 \quad 0\,]^T$ m/s and ${}^{\mathcal{V}}\Delta\boldsymbol{v}_d = [\,4.9992 \quad 0 \quad 0.0873\,]^T$ m/s, respectively. The chief sail is released first, followed by the deputy after a buffer time to further reduce the chance of a close approach immediately after the deployment. The importance of the order in which the sails are released is explained in Sec. V. During the next three orbits, the sails deploy their reflective surfaces and achieve the desired sun-pointing mission attitude. The three-orbit coasting time allows the ground segment to perform orbit and attitude determination before establishing the desired natural formation. The postdeployment coasting period is necessary in order to power up the SEP system using the solar cells, though the coasting duration may vary. To determine the effects of the sails' deployment on the orbit, Gauss's variation-of-parameters equations are used. Because the sails are deployed along the velocity direction, there is no out-of-plane variations. Therefore, the three main orbital elements that change after deployment are [16]

$$\Delta a = \frac{2a^2 v}{\mu}\Delta v_v \tag{8a}$$

$$\Delta e = \frac{1}{v}\left[\frac{r}{a}\sin f\Delta v_b + 2(e+\cos f)\Delta v_v\right] \tag{8b}$$

$$\Delta\omega = \frac{1}{ev}\left[-\left(2e+\frac{r}{a}\right)\cos f\Delta v_b + 2\sin f\Delta v_v\right] - \frac{r\sin\theta\cos i}{h\sin i}\Delta v_h \tag{8c}$$

where $\theta = \omega + f$. For the chief sail that is released first at the orbit perigee, the changes in the orbital elements are $\Delta a_c \approx 1236.67$ km, $\Delta e_c \approx 0.005075$, and $\Delta\omega_c \approx 0$ deg. In this case, the buffer time selected is 25 min. This buffer time directly affects the differential orbital elements postdeployment and, consequently, affects the finite burn for establishing the formation. Therefore, the deployment buffer time may be used as a knob to turn for the establishment of a particular formation size. Releasing the deputy after 25 min leads to the deployment taking place at the true anomaly of $f \approx 3.5$ deg. Using Eq. (4), the changes in the deputy's a, e, and ω are $\Delta a_d \approx 1235.97$ km, $\Delta e_d \approx 0.005071$, and $\Delta\omega_d \approx 0.021$ deg. The corresponding differential orbital elements immediately after deployment are summarized in Table 1. To establish the desired natural formation proposed in Eq. (5), δa, δe, and $\delta\omega$ must vanish at orbit apogee.

V. Establishment of Natural Leader–Follower Formation

Formation establishment is a constrained TPBVP for a hybrid sail solar sail system because of the SEP systems' inability to generate thrust in the direction of the sail's reflective surface. As described in Eq. (5), the desired formation is achieved upon nullifying the differential elements according to $\delta\mathfrak{E} = [\,0 \quad 0 \quad 0 \quad 0 \quad 0 \quad \delta f\,]^T$ at the orbit apogee. The main elements that require adjustment for establishing the desired formation are a, e, and ω since the deployment takes place within the orbit plane. Although the main goal is to nullify δa, δe, and $\delta\omega$, there is a small variation in δi because of lunar–solar effects, and it must be corrected for establishing the desired formation. Furthermore, the sails may not be inserted into the same exact orbit plane as designed nominally, causing variations in δi and $\delta\Omega$. For these reasons, the relative out-of-plane motion must be corrected, even though the corrections are small relative to the corrections required for nullifying the in-plane differential elements. The variation in $\delta\Omega$ is negligible. Therefore, only δi is nullified for correcting the relative out-of-plane motion in solving the TPBVP. Although it is important to nullify all five differential elements mentioned to achieve the proposed natural formation, two differential elements are more important than the others, namely, δa and $\delta\omega$. The identity $\delta a \equiv 0$ must hold for any bounded relative motion, such as the proposed natural formation. A nonzero δa causes the formation to drift apart due to each spacecraft having a different orbit period. Achieving $\delta a \equiv 0$ may not be possible in reality, but $|\delta a|$ must be minimized to have a quasi-periodic relative motion. For the selected burn locations in this Note, only $\delta\omega > 0$ can be nullified without violating the SEP physical constraint. This is explained in more detail in Sec. V.A.

Table 1 Postdeployment differential element

Differential element	Value
δa, km	-0.7
δe	-4.24×10^{-6}
$\delta\omega$, deg	$+0.021$

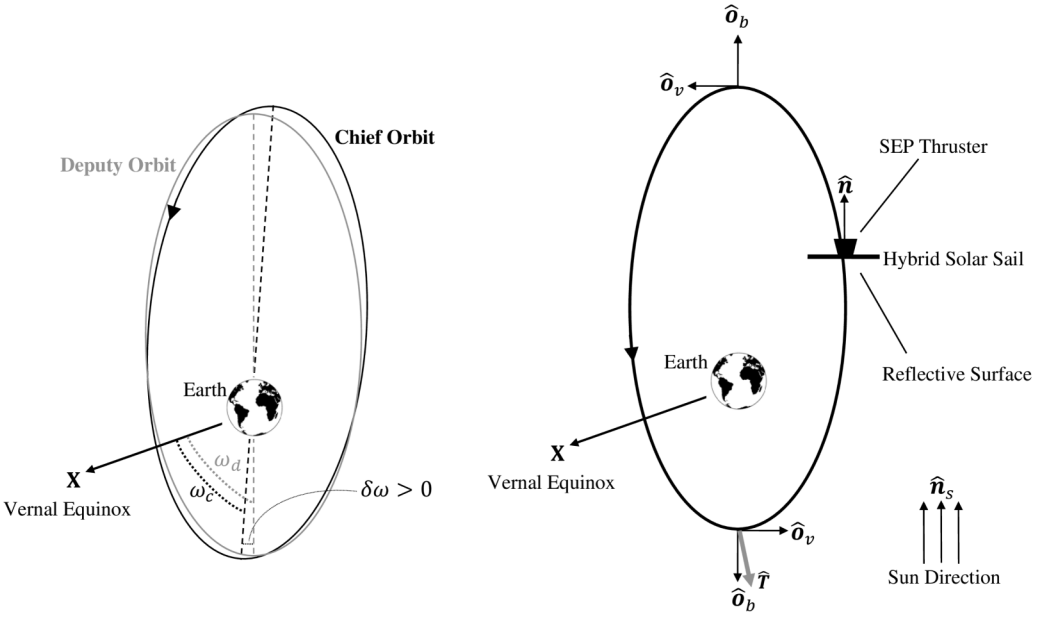

a) Postdeployment orbit configuration **b) Unit burn direction $\hat{T}$ in the deputy's local frame $\mathcal{V}$**

Fig. 4 Sign of $\delta\omega$ after deployment and the direction of burn in the one-burn strategy.

Two solutions are proposed for solving the constrained TPBVP. In the first solution, a one-burn maneuver performed at the deputy's perigee is considered. For the second solution, the first burn is performed at the deputy's perigee, and the second burn is performed at the deputy's apogee. To numerically solve the constrained TPBVP, a predictor-corrector procedure is developed in the high-fidelity FreeFlyer mission design software. The deputy's thruster is assumed to generate the constant thrust value of 0.01 N throughout the maneuver. The thruster burn direction is expressed in the deputy's local $\mathcal{V}$ frame. The differential element δf only affects the formation size, and it has no influence on the shape of the relative orbit. Depending on the deployment strategy, enforcing a particular δf value may lead to overconstraining the problem and to the divergence of the predictor-corrector method for the selected number of burns and burn locations in this study. Therefore, the δf is not explicitly included in the predictor-corrector setup.

A. One-Burn Maneuver

Let $\hat{\boldsymbol{T}}$ and Δt denote the finite burn unit direction and duration, respectively. The finite burn starts at the deputy's perigee. Using the predictor-corrector method, $\hat{\boldsymbol{T}}$ and Δt are modified until $\delta\text{œ} = [\delta a \quad \delta i \quad \delta\omega]^T = [0 \quad 0 \quad 0]^T$ is achieved at the next chief's orbit apogee. The differential element δe is not explicitly nullified in the one-burn strategy. As evident from Table 1, the deputy must increase its semimajor axis and eccentricity to nullify the negative values of δa and δe. To increase both the semimajor axis and eccentricity by burning at the orbit perigee, the deputy must burn along the velocity direction (i.e., $\Delta v_v > 0$). The corresponding increase in the apogee radius, as a result of burning along velocity at the perigee, leads to an increase in the deputy's semimajor axis and eccentricity. Note that, depending on the values of the desired a and e and the initial orbit, a one-burn strategy at perigee does not always lead to achieving the desired a and e. In such a case, both the perigee radius and the apogee radius must be adjusted, which requires a two-burn strategy.

The required burn direction at perigee to nullify $\delta\omega$ depends on the sign of postdeployment $\delta\omega$. To correct for the positive $\delta\omega$ value, the deputy must decrease its argument of perigee as illustrated in Fig. 4a. Inspecting Eq. (8c), to have $\Delta\omega < 0$, we must have

$$\Delta v_b > \frac{2a}{2ae + r} \tan f \Delta v_v \tag{9}$$

where $\Delta v_v > 0$ and it is assumed that $\Delta v_h = 0$. Therefore, to decrease the deputy's argument of perigee (i.e., to have $\Delta\omega < 0$) by

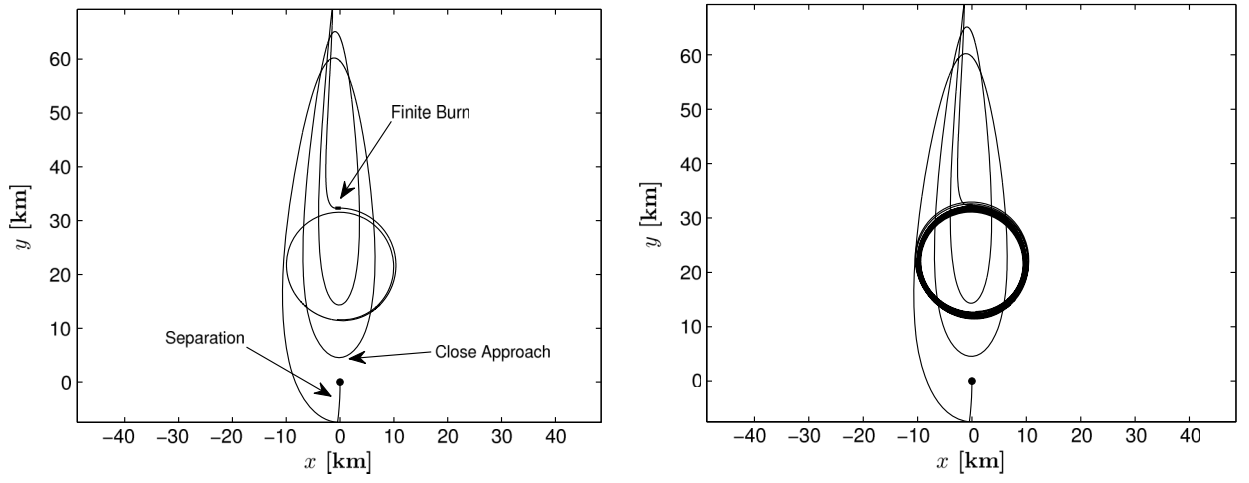

a) Formation establishment via one-burn strategy at perigee **b) 60 days of propagation after formation establishment**

Fig. 5 Deployment and formation establishment as seen in the chief's LVLH frame.

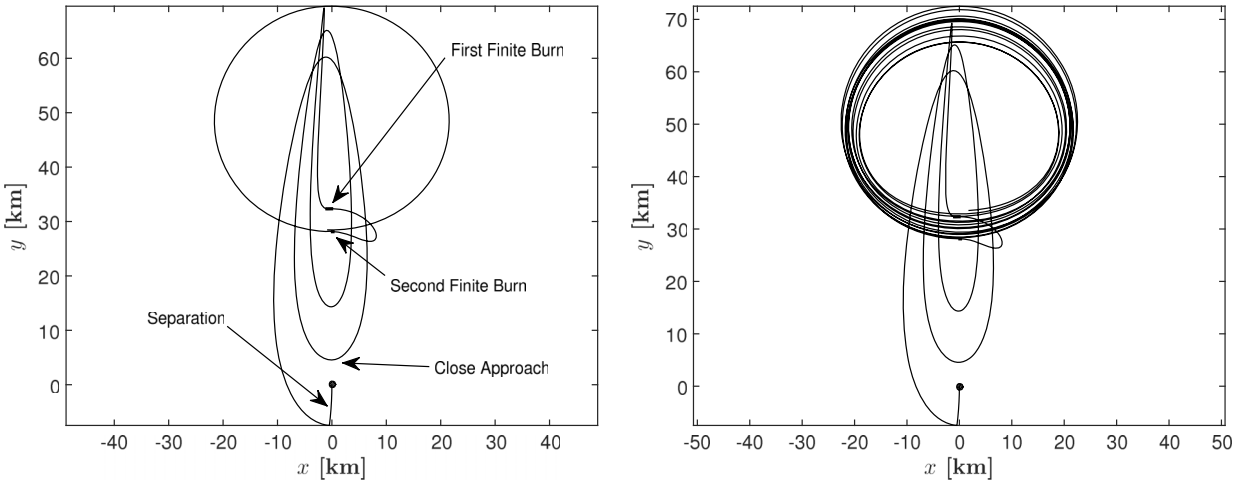

a) Formation establishment via two-burn strategy at perigee and apogee

b) 60 days of propagation after formation establishment

Fig. 6 Deployment and formation establishment as seen in the chief's LVLH frame.

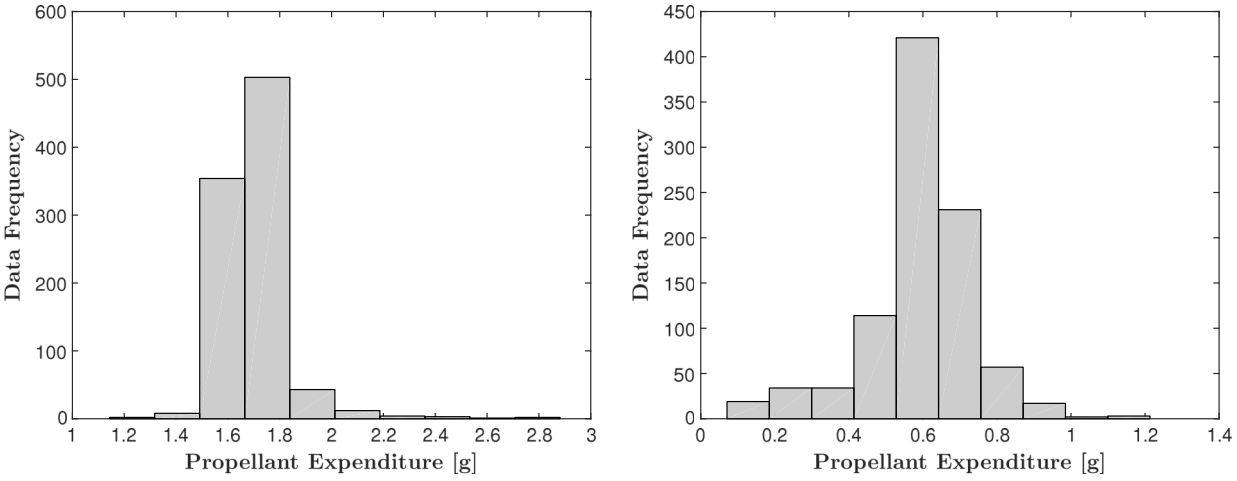

a) First burn propellant expenditure

b) Second burn propellant expenditure

Fig. 7 Histogram for deputy's finite burn duration and propellant expenditure.

burning at perigee, the condition of $\Delta v_b > 0$ must hold. This is the main reason why the chief solar sail is deployed first, because if the order of the deployment is switched, the deputy must then increase its ω to correct for $\delta\omega < 0$. At perigee, this can only be achieved if the deputy executes a radially inward maneuver (i.e., $\Delta v_b < 0$), which violates the SEP system's physical constraint as shown in Fig. 4b. For the deployment scenario considered in Sec. IV, the predictor-corrector method converges to a burn unit direction ${}^{\mathcal{V}}\hat{\boldsymbol{T}} = [\,0.00901 \quad -0.00413 \quad 0.99995\,]^T$ and burn duration of 4011.092 s (≈67 min). As expected, the burn direction is radially outward (along the binormal direction $\hat{\boldsymbol{o}}_b$) and has a positive component along the velocity direction. The nonzero normal component is required to correct for the small nonzero δi that is caused by the lunar–solar perturbations. The net change in velocity is 0.3343 m/s. The total propellant used by the deputy is approximately $\Delta m = 1.64$ g. Figure 5a illustrates the entire scenario consisting of the formation deployment and the establishment of the desired formation using the proposed one-burn maneuver at perigee. As noted earlier, the chief sail is released first along the velocity direction. After 25 min, the deputy sail is released along a direction that is 1 deg off the local velocity direction. Because there is a difference between the orbit periods of the two sails due to nonzero δa, the deputy experiences a secular drift in the along-track direction during the next three orbits before the finite burn begins at the deputy's perigee. To analyze the formation's stability, the established formation is propagated for 60 days as illustrated in Fig. 5b. Despite the presence of the perturbations, the formation remains useful throughout the two-month period.

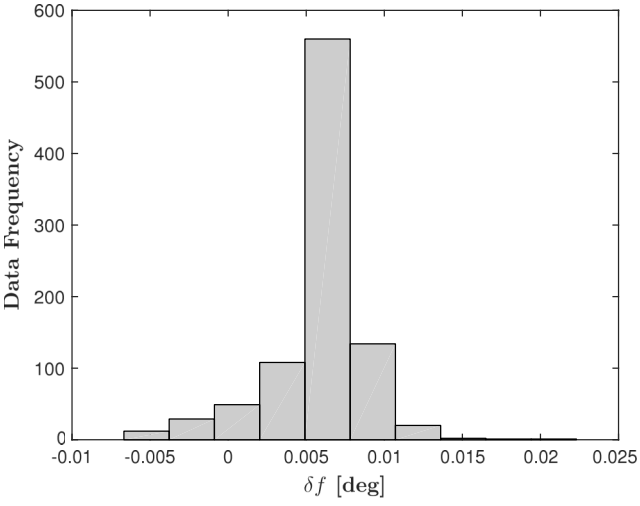

Fig. 8 Histogram for postmaneuver δf values.

B. Two-Burn Maneuver

Typically, changing the orbit semimajor axis and eccentricity requires adjusting both the perigee radius and apogee radius. Thus, a two-burn maneuver may be needed, depending on the postdeployment differential elements. In this case, the first burn is performed at perigee followed by the second burn at apogee. The two-burn strategy allows the deputy to nullify all four nonzero differential elements, namely, δa, δe, δi, and $\delta\omega$. A sample two-burn solution for the same initial condition used in the one-burn scenario is shown in Fig. 6a. The established formation is propagated for 60 days to determine formation stability under perturbations.

As shown in Fig. 6b, the relative trajectory remains quasi-periodic during the 60 day propagation period. Note that the closest approach of 4.6 km occurs at the next perigee, following the deployment of the

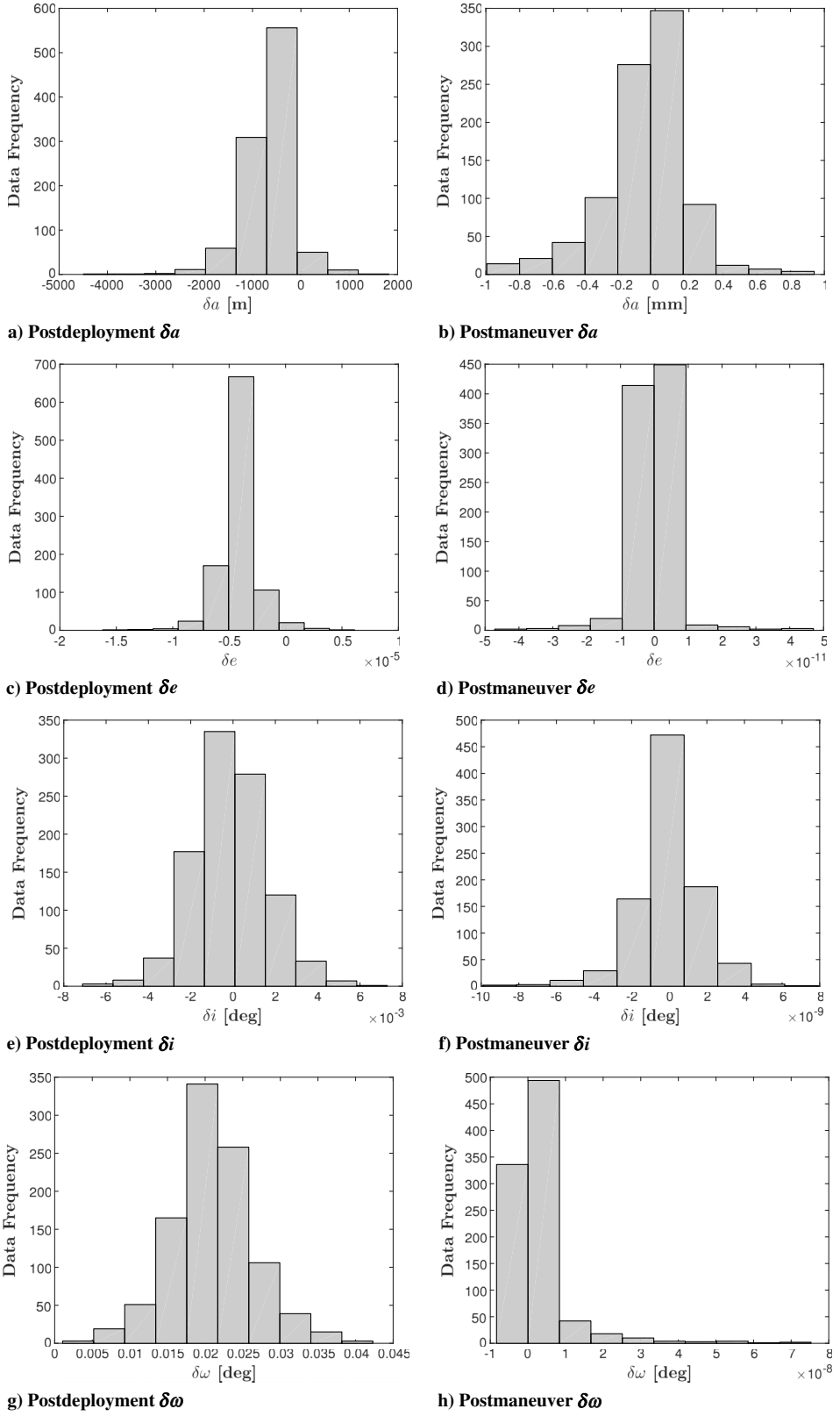

a) Postdeployment δa b) Postmaneuver δa

c) Postdeployment δe d) Postmaneuver δe

e) Postdeployment δi f) Postmaneuver δi

g) Postdeployment $\delta\omega$ h) Postmaneuver $\delta\omega$

Fig. 9 Histograms for postdeployment and postmaneuver differential orbital elements.

deputy sail. The required finite burn unit direction and duration for the first burn at perigee are ${}^{\mathcal{V}}\hat{\boldsymbol{T}}_1 = [0.0125 \quad -0.7161 \quad 0.6979]^T$ and $\Delta t_1 = 4108.741$ s ($\approx$68.5 min). For the second burn at apogee, the finite burn unit direction and duration are ${}^{\mathcal{V}}\hat{\boldsymbol{T}}_2 = [-0.0335 \quad -0.7447 \quad -0.6665]^T$ and $\Delta t_2 = 1444.163$ s ($\approx$24 min). The net velocity changes for the two burns are 0.2571 and 0.0905 m/s, respectively. The propellant expenditures for the first burn and the second burn are approximately $\Delta m_1 = 1.68$ and $\Delta m_2 = 0.59$ g, respectively. Both burn directions satisfy the SEP physical constraint. Inspecting the second component in both burn unit directions, it is clear that the transfer trajectory is an out-of-plane transfer orbit. The maximum out-of-plane point in the transfer trajectory is 3 km.

From the perspective of ground system support, it is best to minimize the number of maneuvers to lower the cost of staffing and expensive communication network coverage. Thus, the one-burn strategy has an advantage over the two-burn strategy in terms of the cost of mission support. Furthermore, the net velocity change for the one-burn maneuver is slightly more efficient than the two-burn maneuver (by approximately 13.3 mm/s). The main drawback of the one-burn maneuver is that it is not always possible to establish the desired formation using a single burn, especially when large errors are introduced during deployment.

VI. Monte Carlo Analysis of Sails Deployment

In this section, a Monte Carlo simulation is performed for the scenario in which the sails are deployed along the local velocity direction with some pointing error. The main purpose of this analysis is to assess the solution space for solving the constrained TPBVP of formation establishment when the sails are deployed in slightly perturbed directions than nominally planned. Additionally, since not every formation size is attainable for a given deployment strategy (δf is not enforced), it is crucial to determine what formation size is achievable for a perturbed deployment scenario. This is to minimize the chance of causing dangerous close approaches after deployment. Because the springs are assumed to be identical, only the direction of the deployment is perturbed; the magnitude of the modelled impulsive burn is kept unchanged for both sails. To perturb the direction along which the sails are deployed, a cone error model is used to apply the maneuver direction error. In this error model, the perturbed maneuver direction creates a cone centered about the nominal direction. Let ${}^{\mathcal{V}}\Delta\boldsymbol{v}$ be the deployment nominal impulsive burn expressed in the $\mathcal{V}$ frame. A $\mathcal{D}$ frame based on the nominal burn ${}^{\mathcal{V}}\Delta\boldsymbol{v}$ is defined as follows:

$$ {}^{\mathcal{V}}\hat{\boldsymbol{d}}_1 = {}^{\mathcal{V}}\Delta\hat{\boldsymbol{v}} = \frac{\Delta\boldsymbol{v}}{\|\Delta\boldsymbol{v}\|} \tag{10a} $$

$$ {}^{\mathcal{V}}\hat{\boldsymbol{d}}_2 = \frac{\hat{\boldsymbol{d}}_1 \times \hat{\boldsymbol{o}}_h}{\|\hat{\boldsymbol{d}}_1 \times \hat{\boldsymbol{o}}_h\|} \tag{10b} $$

$$ {}^{\mathcal{V}}\hat{\boldsymbol{d}}_3 = \hat{\boldsymbol{d}}_2 \times \hat{\boldsymbol{d}}_1 \tag{10c} $$

Thus, the direction cosine matrix $[\mathcal{VD}] = [{}^{\mathcal{V}}\hat{\boldsymbol{d}}_1 \quad {}^{\mathcal{V}}\hat{\boldsymbol{d}}_2 \quad {}^{\mathcal{V}}\hat{\boldsymbol{d}}_3]$ transfers a vector from the $\mathcal{D}$ frame to the $\mathcal{V}$ frame. A perturbed burn direction is created using two consecutive rotations of the nominal $\Delta\boldsymbol{v}$ vector through the cone angle ϵ and the clock angle ψ. Let $\mathcal{E}$ denote the frame that the perturbed burn direction is expressed in after two consecutive rotations are applied to the nominal burn direction $\Delta\hat{\boldsymbol{v}}$. The direction cosine matrix used to perturb the nominal burn direction is $[\mathcal{ED}] = [\boldsymbol{C}_2(\boldsymbol{\epsilon})][\boldsymbol{C}_1(\psi)]$. Thus, the perturbed burn vector $\Delta\boldsymbol{v}_p$ expressed in the local $\mathcal{V}$ frame is written as

$$ {}^{\mathcal{V}}\Delta\boldsymbol{v}_p = \|\Delta\boldsymbol{v}\|[\mathcal{VD}][\mathcal{ED}]^{T\,\mathcal{E}}\Delta\hat{\boldsymbol{v}} \tag{11} $$

where ${}^{\mathcal{E}}\Delta\hat{\boldsymbol{v}} = \hat{\boldsymbol{\epsilon}}_1 = [1 \quad 0 \quad 0]^T$. The clock angle ψ is randomly chosen using a uniform distribution between zero to 360 deg. The cone angle ϵ is randomly selected using a Gaussian distribution with a zero mean and range of 3 deg (3σ). The number of samples for this Monte Carlo analysis is set to 1000 cases. For 83% of the cases run, the numerical solver converges to a solution with burn directions satisfying the physical constraint of the SEP system. Out of the 170 failed cases, 68 cases fail due to the divergence of the predictor-corrector method. The remaining failed cases are due to the predictor-corrector method converging to maneuver plans that violate the maneuver direction constraint. The histograms in Fig. 7 show the postdeployment and the postmaneuver values of the differential orbital elements δa, δe, δi, and $\delta\omega$. In both cases, the formation is propagated to the apogee before reporting the orbital elements. As shown in Fig. 7a, the mean δa postdeployment is approximately 500 m with a maximum difference δa of 2.1 km. As evident in Fig. 7b, the δa values have converged to only a few millimetres after the two-burn maneuver. On average, the burn duration for first finite burn is 69.2 min, while the average for the second finite burn is 24.2 min. The corresponding propellant usage for each burn is shown in Figs. 8a and 8b. The average propellant usages for first and second burns are $\Delta m_1 = 1.69$ and $\Delta m_2 = 0.59$ g, respectively.

As mentioned earlier, δf is not included in the predictor-corrector solver. Therefore, δf may take on a wide range of values. Figure 9 shows the histogram for δf values for all the cases in which the predictor-corrector method converges to a solution. For 812 cases out of the 830 valid solutions, the $|\delta f| > 0.001$ deg, which indicates a safe formation size since $|y_{\min}| = 3.4$ km for $|\delta f| = 0.001$ deg. As can be seen from the center of the histogram, most cases end up with $\delta f \approx +0.005$ deg, which corresponds to a formation with a center at $(x_0, y_0) = (0, +31.7)$, a radius of $R = 14.9$ km, and a closest approach of $y_{\min} = +16.7$ km.

VII. Conclusions

A natural in-plane leader–follower formation is proposed for GEOSAIL mission formation flying using hybrid solar sails that combine solar sailing with a solar electric propulsion (SEP) system. The main advantage of a natural formation is that it only requires the sails to maintain a simple sun-pointing steering law upon establishment of the desired formation. Another advantage of the natural formation is the fact that both small and large formations are achievable. Because the SEP system is only used for the purpose of establishing the formation, only a small and light SEP system is required. It is shown that the desired formation may be established via a modest 0.01 N SEP thruster with an I_{SP} of 2500 s. The constrained two-point boundary value problem of formation establishment is numerically solved using two low-thrust maneuver strategies taking place at perigee and apogee shortly after injection into the GEOSAIL mission orbit. A Monte Carlo analysis is performed to assess the solution space for the formation establishment problem when the sails are injected into slightly different mission orbits due to launch vehicle upper-stage pointing error. It is shown that the natural formation may be established more than 83% of the time even when the sails are injected into slightly different mission orbits.

References

[1] McInnes, C. R., MacDonald, M., Angelopolous, V., and Alexander, D., "GeoSail: Exploring the Geomagnetic Tail Using a Small Solar Sail," *Journal of Spacecraft and Rockets*, Vol. 38, No. 12, 2001, pp. 622–629. doi:10.2514/2.3727

[2] Macdonald, M., Hughes, G., McInnes, C., Lyngvi, A., Falkner, P., and Atzei, A., "GeoSail: An Elegant Solar Sail Demonstration Mission," *Journal of Spacecraft and Rockets*, Vol. 44, No. 12, 2007, pp. 784–796. doi:10.2514/1.22867

[3] Macdonald, M., and McInnes, C., "Analytical Control Laws for Planet-Centered Solar Sailing," *Journal of Guidance, Control, and Dynamics*, Vol. 28, No. 5, 2005, pp. 1038–1048. doi:10.2514/1.11400

[4] Curtis, S., "The Magnetospheric Multiscale Mission: Resolving Fundamental Processes in Space Plasmas," NASA Goddard Space Flight Center TM2000-209883, Dec. 1999.

[5] Gong, S., Yunfeng, G., and Li, J., "Solar Sail Formation Flying on an Inclined Earth Orbit," *Acta Astronautica*, Vol. 68, No. 1, 2011, pp. 226–239.
doi:10.1016/j.actaastro.2010.08.022

[6] Mu, J., Gong, S., and Li, J., "Reflectivity-Controlled Solar Sail Formation Flying for Magnetosphere Mission," *Aerospace Science and Technology*, Vol. 30, No. 1, 2013, pp. 339–348.
doi:10.1016/j.ast.2013.09.002

[7] Mu, J., Gong, S., and Li, J., "Coupled Control of Reflectivity Modulated Solar Sail for GeoSail Formation Flying," *Journal of Guidance, Control, and Dynamics*, Vol. 38, No. 12, 2015, pp. 740–751.
doi:10.2514/1.G000117

[8] Parsay, K., and Schaub, H., "Designing Solar Sail Formations in Sun-Synchronous Orbits for Geomagnetic Tail Exploration," *Acta Astronautica*, Vol. 107, No. 18, 2015, pp. 218–233.
doi:10.1016/j.actaastro.2014.11.018

[9] Yamaguchi, T., Ikeda, H., Mimasu, Y., Tsuda, Y., Takeuchi, H., and Yoshikawa, M., "Hybrid Estimation of Solar Radiation Pressure for a Spinning Solar Sail Spacecraft," *Journal of Spacecraft and Rockets*, Vol. 51, No. 1, 2014, pp. 381–384.
doi:10.2514/1.A32387

[10] Ceriotti, M., and McInnes, C. R., "Systems Design of a Hybrid Sail Pole-Sitter," *Advances in Space Research*, Vol. 48, No. 11, 2011, pp. 1754–1762.
doi:10.1016/j.asr.2011.02.010

[11] Heiligers, J., Ceriotti, M., McInnes, C. R., and Biggs, J. D., "Displaced Geostationary Orbit Design Using Hybrid Sail Propulsion," *Journal of Guidance, Control, and Dynamics*, Vol. 34, No. 6, 2011, pp. 1852–1866.
doi:10.2514/1.53807

[12] Kitamura, S., Ohkawa, Y., Hayakawa, Y., Yoshida, H., and Miyazaki, K., "Overview and Research Status of the JAXA 150-mN Ion Engine," *Acta Astronautica*, Vol. 61, No. 1, 2007, pp. 360–366.
doi:10.1016/j.actaastro.2007.01.010

[13] Schaub, H., and Junkins, J. L., *Analytical Mechanics of Space Systems*, AIAA Education Series, 2nd ed., AIAA, Reston, VA, 2009, pp. 673–753.

[14] Schaub, H., "Relative Orbit Geometry through Classical Orbit Element Differences," *Journal of Guidance, Control, and Dynamics*, Vol. 27, No. 5, 2004, pp. 839–848.
doi:10.2514/1.12595

[15] Williams, T., "MMS Separation and Commissioning Phase Maneuvers," *Advances in the Astronautical Sciences*, Vol. 135, No. 1, 2009, pp. 375–394.

[16] Battin, R. H., *An Introduction to the Mathematics and Methods of Astrodynamics*, AIAA Education Series, rev. ed., AIAA, Reston, VA, 1999, pp. 471–512.